J Mater Sci (2021) 56:1673–1684

Materials for life sciences

Fabrication of strontium-substituted hydroxyapatite scaffolds using 3D printing for enhanced bone regeneration

Hyun-Woo Kim[1] and Young-Jin Kim[1,*]

[1] *Department of Biomedical Engineering, Daegu Catholic University, Gyeongsan 38430, Republic of Korea*

Received: 26 June 2020
Accepted: 24 September 2020
Published online: 6 October 2020

ABSTRACT

The use of porous three-dimensional (3D) bioceramic scaffolds to facilitate the regeneration of bone defects has attracted great attention because their structures closely mimic the natural extracellular matrix. 3D printing is a versatile method for the fabrication of 3D scaffolds. In this study, 3D strontium-substituted hydroxyapatite (Sr-HA) bioceramic scaffolds were prepared by simple precipitation and 3D printing method. The resulting scaffolds exhibited interconnected microporous structures of strands and a single-phase crystal due to HA, meaning that no changes in the phase composition and microstructure of the scaffolds with the Sr content were observed. However, their dissolution rate and biological performance were substantially influenced by changes in the Sr content of the scaffolds. The optimal Sr content in the Sr-HA scaffolds for enhanced proliferation and differentiation of cells were identified by comparing four compositions of the Sr-HA scaffolds. The results of in vitro bioactivity tests demonstrated that the Sr5-HA scaffold with 0.05 of Sr/(Ca + Sr) molar ratio promoted more rapid cell proliferation, osteogenic differentiation, and cellular mineralization compared with the other scaffolds. Therefore, Sr-HA scaffolds have the potential for application in bone regeneration as new bone graft substitutes.

Introduction

The repair of bone defects originating from trauma, tumor resection, and bone diseases demands additional functional components to promote bone regeneration [1]. The reconstruction of bone defects is a complex biological process that requires proper biomaterials, precursor cells, and growth factors [1, 2]. Although autologous bone grafts are regarded as the gold standard for restoring bone defects, alternative materials are needed for the treatment of

Handling Editor: Annela M. Seddon.

Address correspondence to E-mail: yjkim@cu.ac.kr

https://doi.org/10.1007/s10853-020-05391-y

large dimensional bone defects because of the limitations associated with autologous bone grafting, such as donor site morbidity and low graft availability [2, 3]. Hence, tissue-engineered functional biomaterials are currently recognized as the most promising substitutes for autologous bone grafts.

The increasing need for bone grafts has led to the development of alternatives such as synthetic biomaterials [4]. Among various biomaterials, synthetic hydroxyapatite (HA)-based bioceramics have been successfully tested for bioactivity and are used clinically for the treatment of non-healing bone defects [2, 4, 5]. HA is chemically analogous to the mineral component of hard tissues in natural bones and thus exhibits excellent biocompatibility and bioactivity [4]. However, the dissolution rate of pure HA in the human body after implantation is very slow for the optimal formation of bone tissue, resulting in poor performance of HA implants in the early stage of the implantation [4]. Therefore, various metal ions, such as Mg^{2+}, Cu^{2+}, and Sr^{2+}, have been substituted in HA to improve the biological properties of HA for bone tissue regeneration [1, 2, 6, 7].

Among metal ions, Sr^{2+} has been known to play a key role in bone tissue regeneration processes and is associated with the stimulation of osteoblastic functions, induction of osteogenesis, and inhibition of osteoclastic activity [5, 8]. The mechanism by which Sr^{2+} promotes bone tissue regeneration is by increasing osteoblast-related gene expression and the alkaline phosphatase (ALP) activity of cells and inhibiting the differentiation of osteoclasts [9]. Moreover, after the cellular internalization of Sr^{2+}, it can induce interactions with intracellular signaling molecules, such as bone morphogenetic protein 2 (BMP2), to enhance and synergize their biological functions [10]. For these reasons, strontium (Sr)-substituted HA (Sr-HA) has been synthesized using various protocols [11–13]. In addition, various methods, such as compression and gel casting, have been developed for fabricating Sr-HA bioceramic scaffolds [2, 5]. However, no studies have attempted to fabricate Sr-HA bioceramic scaffolds using a three-dimensional (3D) printing technique. This technique can be used to fabricate porous scaffolds with conveniently controllable shape, and thus has been widely used in the fields of bone tissue engineering [13, 14].

Compared with two-dimensional (2D) dense scaffolds, porous 3D scaffolds have attracted much attention because their structures closely resemble the natural extracellular matrix (ECM) [3]. In addition, the presence of Sr in the crystal structure of HA significantly improved cell adhesion, cell proliferation, and osteogenic properties [15]. Therefore, we developed a simple precipitation method for preparing Sr-HA nanoparticles and a 3D printing method for fabricating 3D Sr-HA bioceramic scaffolds to support bone tissue regeneration. The effect of Sr content on the structure, physicochemical properties, and ion release behavior of the fabricated Sr-HA scaffolds was evaluated. Furthermore, their biological activity was investigated through in vitro studies, such as cell proliferation, ALP activity, osteoprotegerin (OPG) expression, and cellular mineralization assays.

Materials and methods

Materials

Calcium nitrate tetrahydrate ($Ca(NO_3)_2{\cdot}4H_2O$), strontium nitrate ($Sr(NO_3)_2$), ammonium phosphate dibasic ($(NH_4)_2HPO_4$), ammonium hydroxide solution (25 w/v%, NH_4OH), sodium alginate, 3-(4,5-dimethylthiazol-2-yl)-2,5-diphenyltetrazoliumbromide (MTT), alizarin red S (ARS), and cetylpyridinium chloride were purchased from Sigma-Aldrich Co. (St. Louis, MO, USA) and used as received. Poly(vinyl alcohol) (PVA) binder (HS-BD25) and polycarboxylic acid-type dispersant (HS-DISPERSANT5803) were obtained from San Nopco Korea (Seoul, Republic of Korea) and used without further purification. A mouse calvaria preosteoblast cell line (MC3T3-E1) was obtained from the American Type Culture Collection (ATCC, Manassas, VA, USA). Alpha minimum essential medium (α-MEM), fetal bovine serum (FBS), penicillin–streptomycin, and Dulbecco's phosphate-buffered saline (DPBS, pH 7.4) were purchased from Gibco BRL (Waltham, MA, USA). SlowFade Gold antifade mountant and the LIVE/DEAD Viability/Cytotoxicity Assay Kit were obtained from Molecular Probes (Eugene, OR, USA). The Actin Cytoskeleton and Focal Adhesion Staining Kit was purchased from Merck Millipore (Burlington, MA, USA). The Mouse Osteoprotegerin enzyme-linked immunosorbent assay (ELISA) Kit was purchased from Biomatik (Wilmington, DE, USA). All

other reagents and solvents were obtained from commercial sources and used as received.

Synthesis of Sr-HA nanoparticles

Sr-HA nanoparticles were synthesized as follows. A determined amount ((Ca + Sr)/P = 1.67) of 0.1 M $(NH_4)_2HPO_4$ solution (pH 10) was added dropwise into mixed aqueous solutions (pH 10) of 0.1 M $Ca(NO_3)_2{\cdot}4H_2O$ and 0.1 M $Sr(NO_3)_2$ containing 0.03 w/v% sodium alginate over a period of 2 h. Sr/(Ca + Sr) molar ratios in the reactant solutions were 0, 0.02, 0.05, and 0.1. The mixtures were vigorously stirred at 45 °C for 24 h to induce the nucleation and growth of Sr-HA crystals in the alginate matrix. The resultant nanoparticles were then isolated by centrifugation and washed with distilled water (DW) in three replicates, followed by lyophilization in vacuo. The obtained products were named Sr0-HA, Sr2-HA, Sr5-HA, and Sr10-HA nanoparticles.

Fabrication of 3D Sr-HA scaffolds

The fabrication of Sr-HA bioceramic scaffolds was performed with a 3D printing machine (ROKIT INVIVO, Rokit Healthcare, Seoul, Republic of Korea). Before 3D printing the Sr-HA scaffolds, synthesized Sr-HA nanoparticles (20 g) were mixed with a PVA binder (2 g), polycarboxylic acid-type dispersant (2 g), and DW (6 g). The mixture was transferred to a stainless syringe. Then, the disk-shaped scaffolds designed by a Solidworks CAD software (Dassault Systemes Solidworks Corp., Vélizy-Villacoublay, France) were 3D-printed under the conditions of a 10 mm/s nozzle moving speed and 600 kPa pneumatic pressure at room temperature. After 3D printing, the scaffolds were freeze-dried, followed by thermal treatment at 1150 °C for 3 h to burn out polymeric materials, such as sodium alginate, PVA binder, and polycarboxylic acid-type dispersant. The dimension of final bioceramic scaffolds was fixed at a 10 mm diameter and 2 mm thickness. The fabricated samples were named Sr0-HA, Sr2-HA, Sr5-HA, and Sr10-HA scaffolds.

Morphology and physicochemical properties of 3D Sr-HA scaffolds

The morphologies of Sr-HA scaffolds were observed by scanning electron microscopy (SEM, S-4300, Hitachi, Tokyo, Japan) after sputter-coating of samples with platinum. For the same samples used in SEM, energy-dispersive X-ray spectroscopy (EDX) was used to determine the change in the elemental composition of the Sr-HA scaffolds. The chemical compositions of the samples were determined by Fourier transform infrared spectroscopy (FTIR) using an ALPHA spectrometer (Bruker Optics, Billerica, MA, USA) in attenuated total reflectance (ATR) mode. FTIR spectra were collected in the wavenumber range from 400 to 2200 cm^{-1} with a resolution of 4 cm^{-1}. The crystalline phases of the Sr-HA scaffolds were identified by X-ray diffraction (XRD) analysis using a high-resolution X-ray diffractometer (D/MAX-2500 V/PC, Rigaku, Tokyo, Japan) with Cu Kα radiation (2θ range of 10°–50°). The compressive strengths of the Sr-HA scaffolds were measured using an Instron 5565 universal testing machine (Instron Co., Norwood, MA, USA) using a force load cell of 5 kN capacity. Each scaffold sample was tested 5 times at a loading speed of 5 mm/min.

In vitro ion release measurement from 3D Sr-HA scaffolds

The in vitro cumulative Sr^{2+} ion release from the Sr-HA scaffolds was quantitatively measured for 14 days using an Agilent 7800 Quadrupole inductively coupled plasma mass spectrometry (ICP-MS, Agilent Technologies Inc., Santa Clara, CA, USA). The disk-shaped Sr-HA scaffolds (10 mm diameter and 2 mm thickness) were weighed and immersed in 2 mL DW at 37 °C. The supernatants were collected from the solution at preset time points. The cumulative release amounts of Sr^{2+} ions from the scaffolds were determined in solution after experiments against standard solutions by measuring the adsorption of the samples by ICP-MS. The ion concentration was calculated.

Cell attachment and proliferation assay

The cell proliferation of MC3T3-E1 cells was analyzed to determine the in vitro bioactivity of the Sr-HA scaffolds. All cells sere cultured in α-MEM containing 10 FBS and 5% penicillin–streptomycin at 37 °C with 5% CO_2. The scaffolds were sterilized in an autoclave at 120 °C for 20 min, rinsed thrice each with DPBS and α-MEM, placed into a 48-well tissue culture plate, and fixed with glass ring (inner diameter = 7 mm).

Then, 1 mL of cell suspension (2×10^4 cells/well) was placed onto the sterilized scaffolds, and cells were cultured for different amounts of time. The cell proliferation of MC3T3-E1 cells on the scaffolds was determined using the MTT assay at days 1, 3, 5, 7, and 14. At each time point, the culture medium was mixed with 0.2 mL of the MTT solution (5 mg/mL in DPBS), and the cells were incubated for another 4 h. Next, the remaining medium was removed, and 1 mL of DMSO was added to solubilize the precipitated formazan crystals. Finally, 0.1 mL triplicates from each resulting sample were transferred to a 96-well plate, and the optical density at 570 nm was determined using a microplate reader (OPSYS-MR, Dynex Technology Inc., Chantilly, VA, USA).

To confirm the bioactivity of the Sr-HA scaffolds, the cell viability of MC3T3-E1 cells cultured on the scaffolds was qualitatively analyzed using the LIVE/DEAD Viability/Cytotoxicity Assay Kit according to the manufacturer's instructions. In this assay, calcein AM stains live cells green and ethidium homodimer-1 (EthD-1) stains dead cells red [16]. MC3T3-E1 cells were seeded onto the scaffolds at a density of 2×10^4 cells per well and cultured at 37 °C for 7 days. The cells were stained for 30 min at room temperature with 2 μM of calcein AM and 4 μM of EthD-1, followed by another 1 day incubation. Live cells were observed using a fluorescence microscope (Eclipse TS100, FITC-G2A filters, Nikon, Tokyo, Japan).

Cell attachment and morphologies of MC3T3-E1 cells cultured on the scaffolds were visualized by SEM and confocal laser scanning microscopy. Cells cultured on the Sr-HA scaffolds for 7 days were fixed with 4% glutaraldehyde for 1 h and then washed using DPBS. After dehydrating with a graded series of ethanol, the samples were vacuum-dried, followed by platinum coating for SEM analysis. Other fixed samples were treated with 0.1 w/v% Triton-X 100 for 10 min to permeabilize the cell membrane. The cultured cells were subjected to previous immunocytochemical procedures with tetramethylrhodamine-conjugated phalloidin (phalloidin-TRITC) to stain cytoskeletal F-actin and H-33258 to counterstain the nuclei. Cells were then visualized with an inverted LSM 700 confocal laser scanning microscope (Carl Zeiss, Oberkochen, Germany). As a result, nuclei and F-actin were visualized in blue and red, respectively.

Cell differentiation and cellular mineralization assay

ALP activity is commonly used as an early indicator of osteoblastic differentiation of MC3T3-E1 cells [1]. Therefore, ALP activity was evaluated at 3, 7, 14, and 21 days using a QuantiChrom™ Alkaline Phosphatase Assay Kit (DALP-250, BioAssay Systems, Hayward, CA, USA) based on the hydrolysis of *p*-nitrophenyl phosphate to *p*-nitrophenol. In this assay, the formation of *p*-nitrophenol is proportional to ALP activity. Absorbance was determined at 405 nm using a microplate reader. OPG is known as an osteoclastogenesis inhibitory factor, and its production by osteoblastic cells dictates the rate of osteoclastic bone resorption [17]. The level of OPG expression in cells cultured on the scaffolds was determined by the measuring absorbance at 450 nm using a Mouse Osteoprotegerin ELISA Kit (Biomatik, Wilmington, DE, USA) after 7 days of culture. The OPG concentration was calculated by linear interpolation of the standard curve. The kit was used according to the manufacturer's specification.

The calcium deposition capability of MC3T3-E1 cells cultured on the Sr-HA scaffolds was evaluated by ARS staining because ARS can selectively bind to calcium ions [8]. The cells were cultured on the scaffolds for 14 days and then fixed with 4% glutaraldehyde for 30 min. After staining with 1 mL of ARS (pH 4.2, 40 mM) with gentle agitation for 20 min, the samples were washed thrice with DW. For quantitative analysis, 1 mL of 10% cetylpyridinium chloride (pH 7.0, 10 mM) was added to the culture plate to elute the stains for 30 min. The optical density of the supernatant was determined at 540 nm using a microplate reader.

Statistical analysis

All data were expressed as the mean value ± standard deviation from at least 4 independent experiments. Differences between 2 groups were analyzed with a one-way ANOVA followed by Tukey's test using SigmaPlot 13.0 (Systat Software Inc., San Jose, CA, USA). The level of significance was defined for values of $p^* < 0.05$ and $p^{**} < 0.01$.

Results and discussion

Fabrication of 3D Sr-HA scaffolds

An ideal scaffold for bone tissue regeneration should support the proliferation of bone-forming cells and offer favorable osteogenic activity to regulate cell responses, resulting in new bone formation [13]. Sr-HA-based bioceramics exhibit better biodegradability and biocompatibility than pure HA-based bioceramics [18]. In the present study, Sr-HA nanoparticles containing different contents of Sr were first synthesized via a one-step precipitation reaction in the presence of alginate and then used to fabricate the 3D Sr-HA scaffolds by 3D printing. The prepared Sr-HA nanoparticles exhibited spherical shapes with a diameter of less than 100 nm (Fig. 1). Their shape and size are due to the strong ionic interaction between the COOH group of alginate and cations (Ca^{2+} or Sr^{2+} ions) [19]. This ionizable side group of alginate is useful for the nucleation of Sr-HA crystals in the solution because the COOH group can provide a site for the selective adhesion of Ca^{2+} or Sr^{2+} ions to form a specific stereochemical arrangement of reactive groups in alginate–Ca^{2+} or alginate–Sr^{2+} complexes. These complexes strongly combine with PO_4^{3-} ions to initiate the nucleation and growth of Sr-HA nanoparticles.

The 3D Sr-HA scaffolds were fabricated using a 3D printing method with mixtures of the synthesized Sr-HA nanoparticles, PVA binder, polycarboxylic acid-type dispersant, and DW, followed by thermal treatment at 1150 °C. The surface morphologies of the Sr-HA scaffolds were observed by SEM and optical imaging. According to the digital camera and SEM images shown in Fig. 2, the micro- and macro-morphologies of the resulting scaffolds were very similar to each other. The surfaces of strands in the Sr-HA scaffolds displayed an interconnected microporous structure consisting of uniform micropores and unequiaxed grains (Fig. 2c). The formation of micropores in the strands of scaffolds is mainly due to the decomposition of polymers and the melting of nanoparticles.

Physicochemical properties of 3D Sr-HA scaffolds

FTIR was used to analyze the chemical structure of Sr-HA scaffolds by identifying the functional groups of the resulting scaffolds. The spectra of all samples exhibited characteristic absorption bands at 1091, 1025, and 961 cm^{-1} corresponding to P–O stretching vibration modes (Fig. 3a) [1, 20]. In addition, the absorption peaks appeared at 632, 602, and 563 cm^{-1} associated with the O–P–O bending vibration modes. However, changes in characteristic bands with Sr

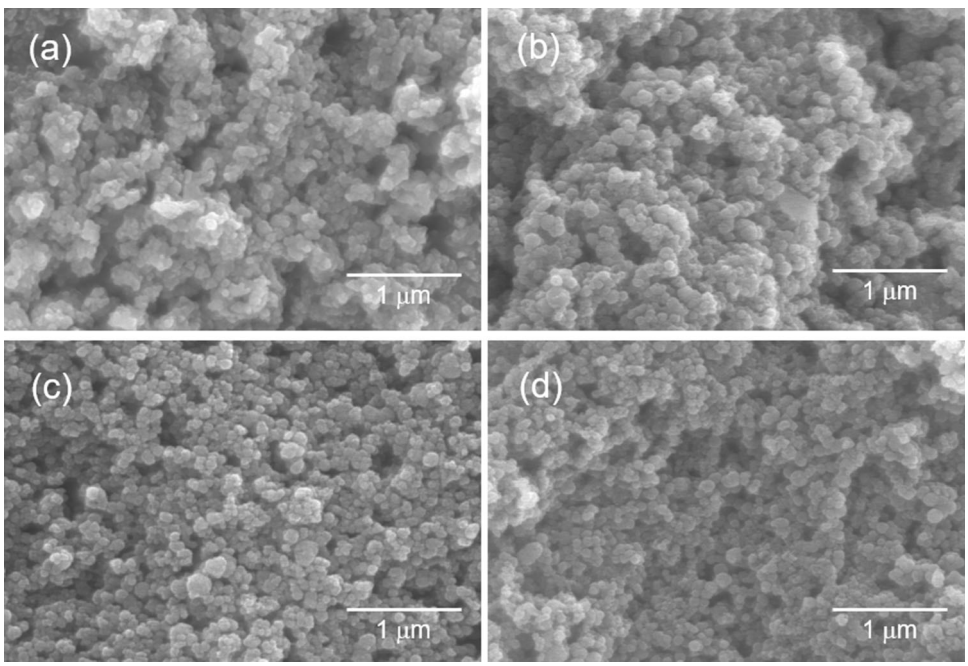

Figure 1 SEM images of **a** Sr0-HA, **b** Sr2-HA, **c** Sr5-HA, and **d** Sr10-HA nanoparticles.

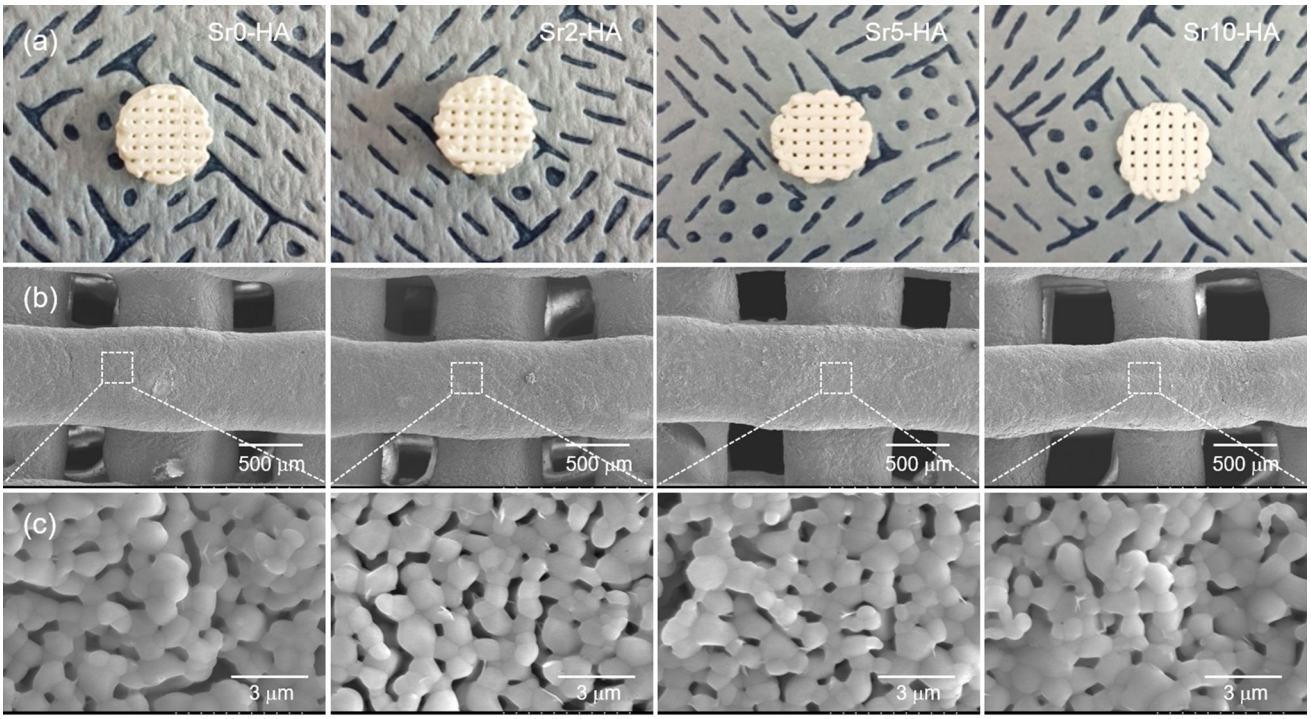

Figure 2 The macro- and micro-morphologies of 3D-printed Sr-HA scaffolds fabricated with Sr-HA nanoparticles containing different contents of Sr: **a** optical and **b, c** SEM images of Sr-HA scaffolds.

Figure 3 **a** FTIR and **b** EDX spectra of the Sr-HA scaffolds.

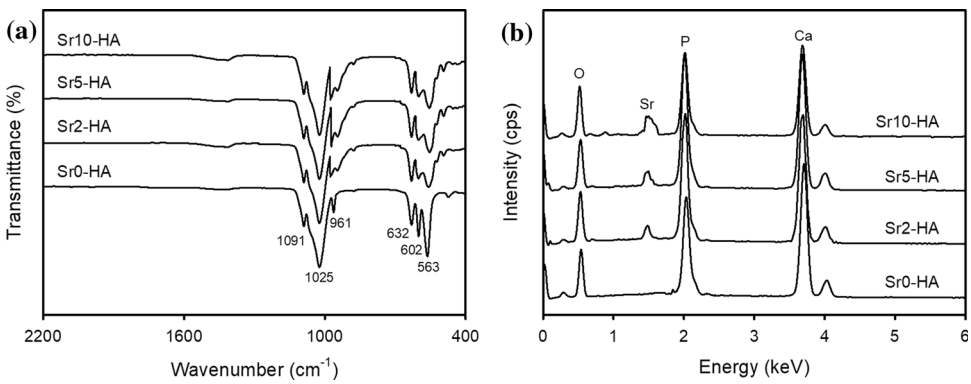

content were not observed. To confirm the fabrication of Sr-HA scaffolds, the surface elemental composition of the scaffolds was examined using EDX. The Sr0-HA scaffold exhibited only three peaks ascribed to O, P, and Ca, as shown in Fig. 3b. However, Sr2-HA, Sr5-HA, and Sr10-HA exhibited a new peak that corresponded to the Sr of Sr-HA crystals. The intensity of the peak assigned to Sr increased with the increasing Sr content in the scaffolds.

The crystalline phases of the Sr-HA scaffolds were assessed by means of XRD (Fig. 4). All samples exhibited typical diffraction patterns that were consistent with the JCPDS database (JCDPDS 09–0432) for the HA crystalline phase. The peaks were attributable to the (200), (111), (002), (102), (210), (211), (112), (300), (202), (310), (311), (113), (222), (312), and (213) reflections of the HA crystal [13, 21]. However, the XRD peaks at the 2θ range of 31 °–33 ° were shifted to a smaller angle with the increasing Sr content (Fig. 4b). This was mainly attributed to the larger ionic radius of Sr^{2+} in the Sr-HA scaffolds [5, 13].

The scaffold should be strong enough to withstand the force during new bone tissue regeneration. Therefore, the mechanical properties of the Sr-HA scaffolds were investigated on the basis of

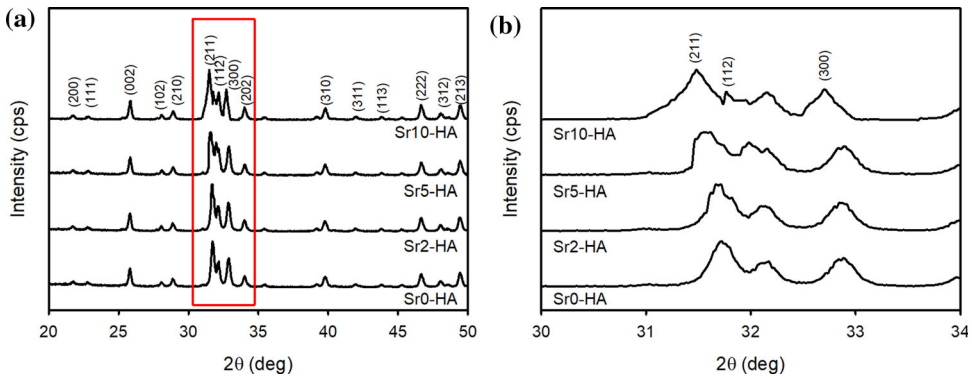

Figure 4 XRD patterns of the Sr-HA scaffolds for **a** 2θ = 20 °–50 ° and **b** 2θ = 30 °–34 °.

compressive strength test. As displayed in Fig. 5, the results obtained from the compressive strength measurements exhibited that the Sr content hardly affected the mechanical properties of the Sr-HA scaffolds.

Cell attachment and proliferation assay

The in vitro bioactivity of the Sr-HA scaffolds was investigated to evaluate the potential of the scaffolds as bone graft substitutes. The proliferation rate of MC3T3-E1 cells cultured on the Sr-HA scaffolds was evaluated by the MTT assay in which higher cell viability indicates better cytocompatibility of the Sr-HA scaffolds. A time-dependent increase in the number of cells was observed for all tested samples except Sr10-HA (Fig. 6a). Changes in the Sr content of the Sr-HA scaffolds significantly influenced cell viability. The Sr-HA scaffolds containing a low content of Sr (Sr0-HA, Sr2-HA, and Sr5-HA) promoted more rapid cell proliferation compared with the scaffold containing a high content of Sr (Sr10-HA). Among the scaffolds, the highest proliferation rate of cells was observed for the Sr5-HA scaffold at all tested time points. These results were associated with the Sr content in the Sr-HA scaffolds and with the dissolution rate of the scaffolds, suggesting that the degree of Sr substitution in the scaffolds affects cell viability.

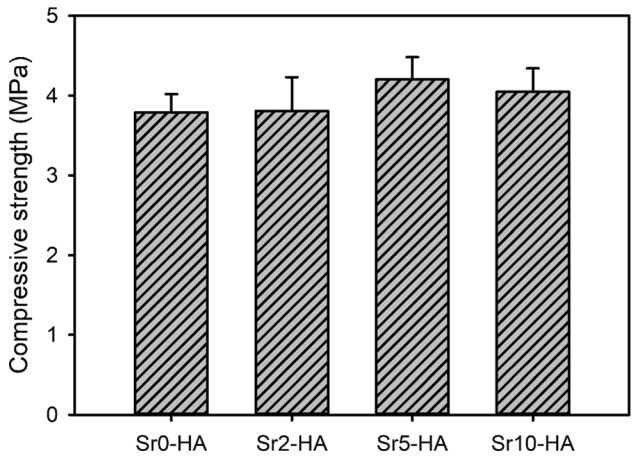

Figure 5 Compressive strength of the Sr-HA scaffolds (n = 5).

It has been previously reported that the solubility and dissolution rate of bioceramics played an important role in the improvement of proliferation and differentiation of osteoblasts [3, 5, 22]. In general, the high open microporous structure of 3D-printed scaffolds accelerates the degradation of scaffolds and ion exchange process because enlargement of the accessible surface of the scaffolds can allow the penetration of water into the scaffolds [3]. Therefore, the release of Sr^{2+} ions from 3D-printed Sr-HA scaffolds during cell culture was simulated by immersion of these scaffolds in α-MEM according to the same conditions of cell culture used to investigate the dissolution rate of the scaffolds.

As shown in Fig. 6b, the Sr-HA scaffolds excepting Sr0-HA fabricated with pure HA exhibited a high dissolution rate, which increased steadily with the increasing Sr content because of the larger ionic radius of Sr^{2+} (113 pm) compared with Ca^{2+} (99 pm) [5]. As a consequence, this enhanced dissolution rate contributed to the high bioactivity of Sr-HA scaffolds [1–5]. However, a higher degree of Sr substitution caused a rapid dissolution of Sr10-HA because of its larger crystal size, leading to a cell detachment from the surface of the scaffold. In addition, rapid degradation of the bioceramic scaffolds can inevitably change the microenvironment through the production of high levels of Ca^{2+} and PO_4^{3-} and consequential change of the local pH, causing a mild inflammatory response [23]. These results suggest

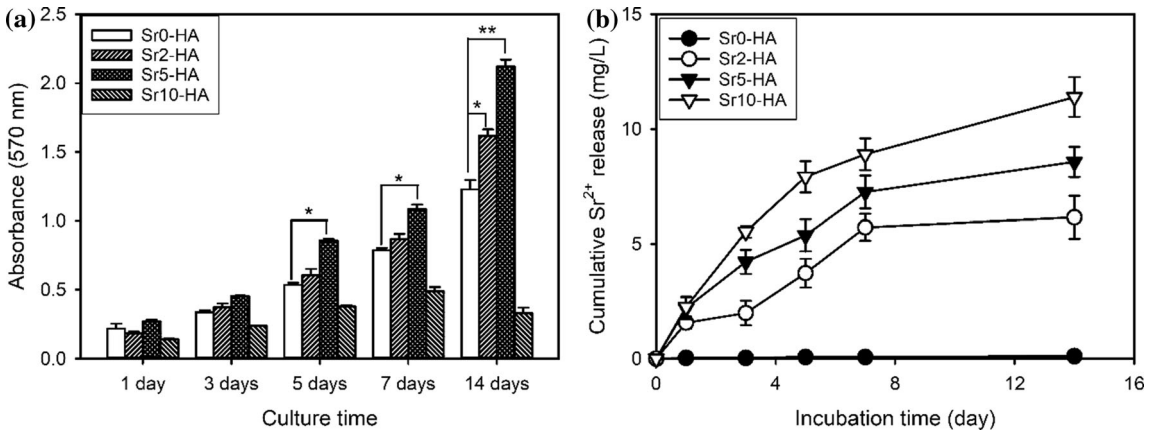

Figure 6 **a** Proliferation of MC3T3-E1 cells cultured on the Sr-HA scaffolds (n = 5) and **b** Sr ion concentration as a function of immersion time in DW for the dissolution of the Sr-HA scaffolds (n = 5). Significant differences from the Sr0-HA scaffold at each time point were denoted as $p^* < 0.05$ and $p^{**} < 0.01$.

that the dissolution rate of the Sr-HA scaffolds can affect cell proliferation.

To qualitatively verify the bioactivity of the Sr-HA scaffolds, MC3T3-E1 cells were seeded on the scaffolds and incubated for 7 days. Cell proliferation was assessed by live-cell staining and observed using a fluorescence microscope (Fig. 7). The viable cells exhibited green fluorescence upon staining with calcein AM. We observed that the cells were successfully attached and proliferated on the surface of strands in the scaffolds, and the highest number of cells was observed on Sr5-HA. This result was consistent with the MTT assay results.

The attachment and morphology of cells were observed to examine cell growth on the Sr-HA scaffolds using SEM after 7 days of culture. SEM images showed that the cells adhered and spread on the surface of strands in the Sr-HA scaffolds (Fig. 8). In addition, cell spreading was also observed on the back of strands, as displayed in cross-sectional images of Fig. 8. Moreover, the cells spread over almost the whole surface of strands in Sr5-HA after culturing

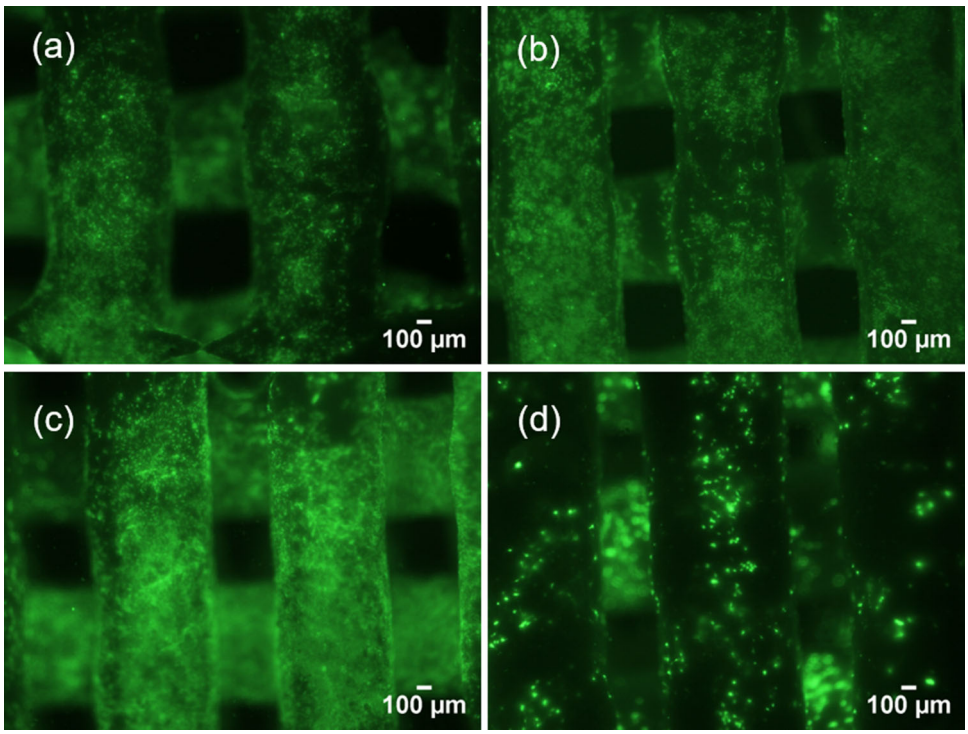

Figure 7 Fluorescence microscopy images of live cells stained with calcein AM (green) after 7 days of cell culture on **a** Sr0-HA, **b** Sr2-HA, **c** Sr5-HA, and **d** Sr10-HA scaffolds.

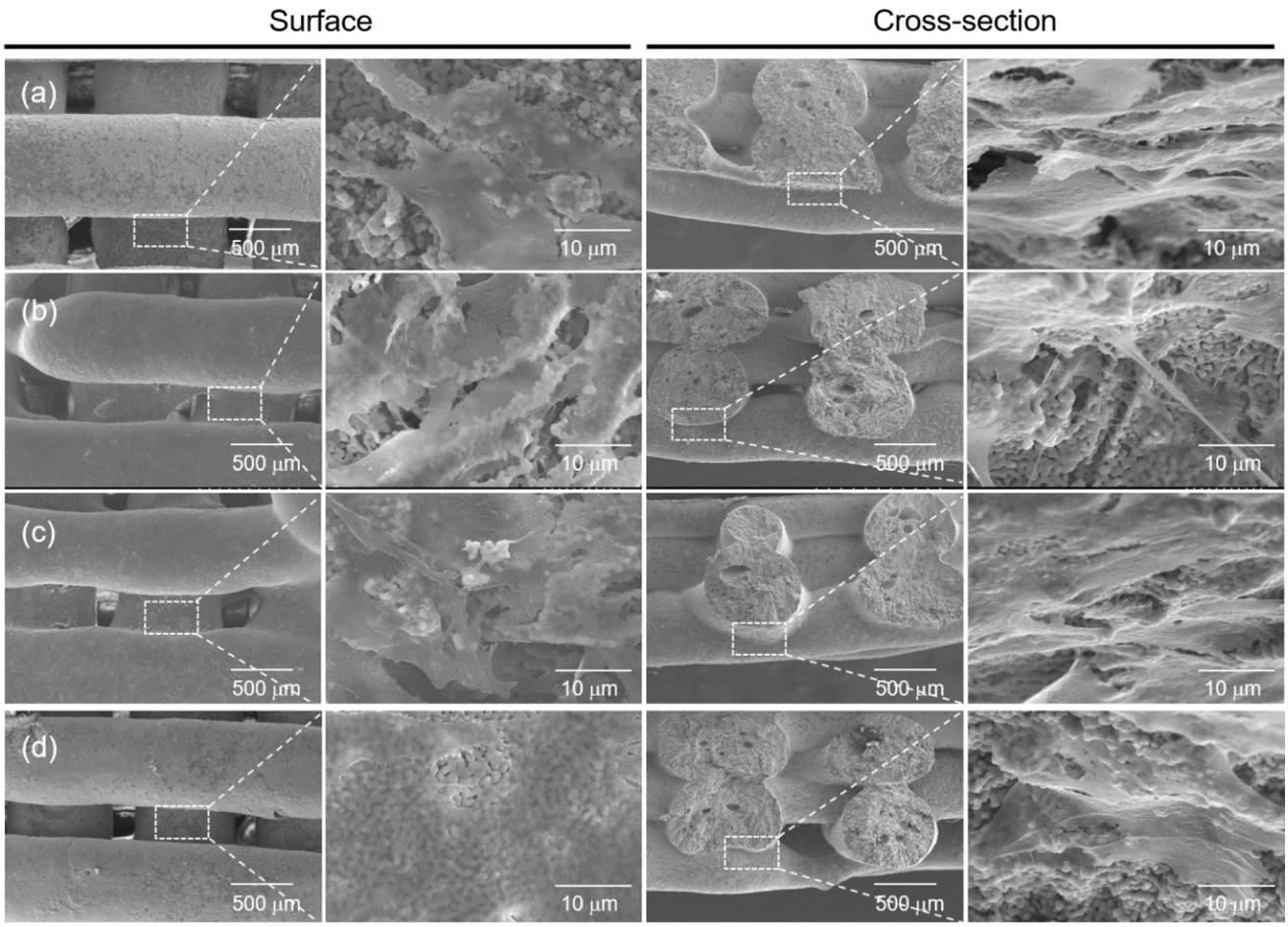

Figure 8 SEM images of cell growth on **a** Sr0-HA, **b** Sr2-HA, **c** Sr5-HA, and **d** Sr10-HA scaffolds after culturing for 7 days.

for 7 days. The spreading of MC3T3-E1 cells on the Sr-HA scaffolds was investigated in detail by analyzing the cytoskeleton. The nuclei and actin filaments of cells were stained using H-33258 (blue) and phalloidin-TRICT (red), respectively. As shown in Fig. 9, spindle cells exhibited a well-stretch morphology characterized by elongated actin filaments. In addition, the cells were uniformly distributed over the surfaces of the strands in all scaffolds. However, the number of stained cells on the Sr5-HA scaffold was higher than on the other scaffolds.

Cell differentiation and cellular mineralization

Osteoblastic differentiation of MC3T3-E1 cells on the Sr-HA scaffolds was examined by measuring ALP activity, an early marker of osteogenic differentiation, because ALP expression affects the formation of bone mineral [2, 3]. A highly significant increase in ALP activity in MC3T3-E1 cells cultured on Sr5-HA was observed at days 14 and 21 compared with the other scaffolds (Fig. 10a). The ALP activity of osteogenic differentiating cells is influenced by cell confluence and interaction with osteoinductive elements on the scaffolds [24]. Therefore, the Sr-HA scaffolds and their ionic release products affected the expression of ALP activity. Specifically, ALP activity increased with the increasing Sr content and dissolution rate of the scaffolds. However, an extremely rapid dissolution rate of the scaffolds induced cytotoxic conditions, cell detachment from the scaffolds, and thereby down-regulated ALP activity. Similar results have been previously reported that Sr^{2+} ions released from the scaffolds stimulated the ALP activity of osteoblasts by accelerating the formation of extracellular matrix [3, 25].

OPG inhibits the binding of receptor activator of nuclear factor κB ligand (RANKL) to receptor activator of nuclear factor κB (RANK). Thus, it can

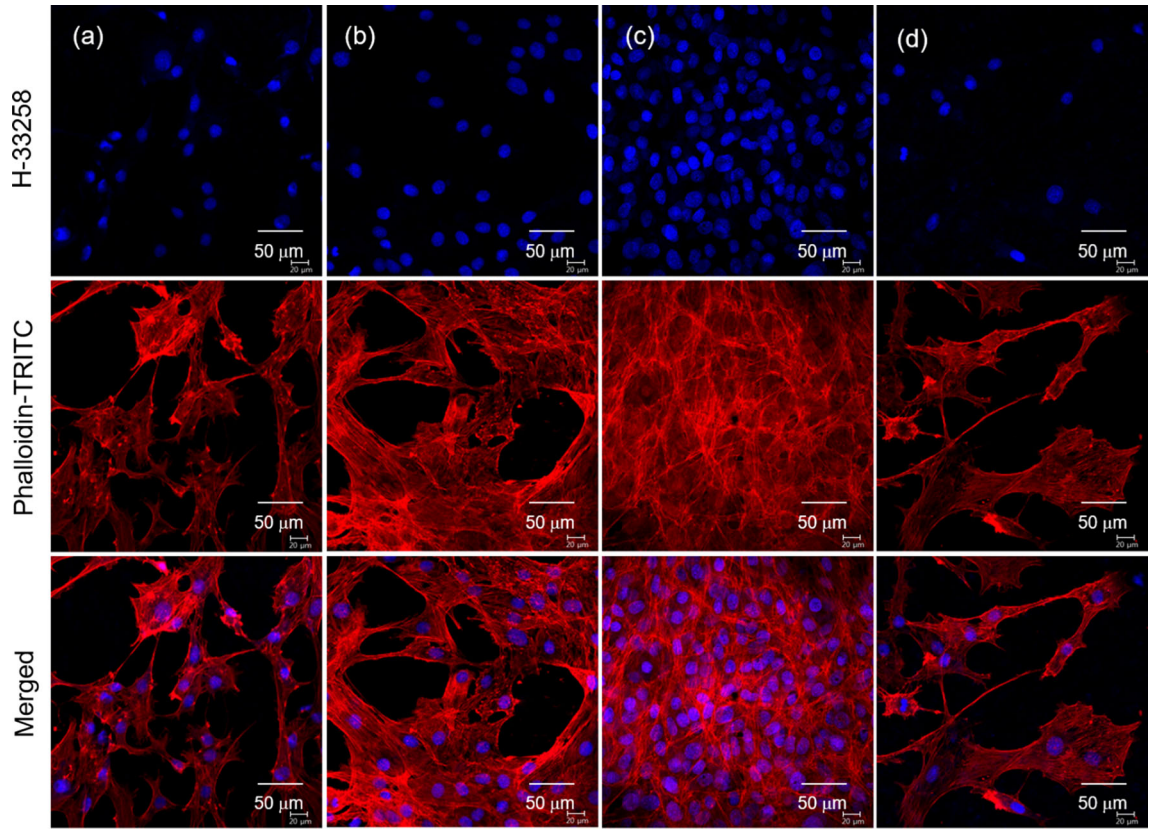

Figure 9 Confocal laser scanning microscopy images of MC3T3-E1 cells grown on **a** Sr0-HA, **b** Sr2-HA, **c** Sr5-HA, and **d** Sr10-HA scaffolds after culturing for 7 days.

inhibit the differentiation, proliferation, and activation of osteoclasts, resulting in the down-regulation of bone resorption in a dose-dependent manner [17, 26]. As displayed in Fig. 10b, Sr5-HA enhanced the upregulation of OPG expression compared with the other scaffolds. This increased OPG expression may increase bone formation and decrease bone resorption.

The ability of osteoblastic cells to deposit bone-like calcium on the Sr-HA scaffolds is generally used as a late-stage marker for osteogenic differentiation. This cellular mineralization can be determined by the ARS method [8]. The absorbance of ARS in the red-stained scaffolds after 14 days of cell culture was used to quantify cellular mineralization. Compared with the other scaffolds, Sr5-HA showed the highest calcium deposition and osteogenesis ability, suggesting the significant role of Sr^{2+} ions in cellular mineralization (Fig. 10c). Therefore, the Sr content of the Sr-HA scaffolds markedly affected osteogenic differentiation and mineralization.

Conclusion

In this study, simple precipitation and 3D printing methods were developed to prepare 3D Sr-HA bioceramic scaffolds for application in bone tissue regeneration. The scaffolds obtained had interconnected microporous structures of strands. The Sr content influenced the physicochemical properties, dissolution rate, and the in vitro bioactivity of the scaffolds, as well as the bone-forming ability of the cells cultured on the Sr-HA scaffolds. Sr5-HA promoted cell proliferation, osteogenic differentiation, and cellular mineralization more efficiently compared with the other scaffolds. From these results, our simple method for fabricating the Sr-HA scaffolds may contribute to the development of new bone graft substitutes.

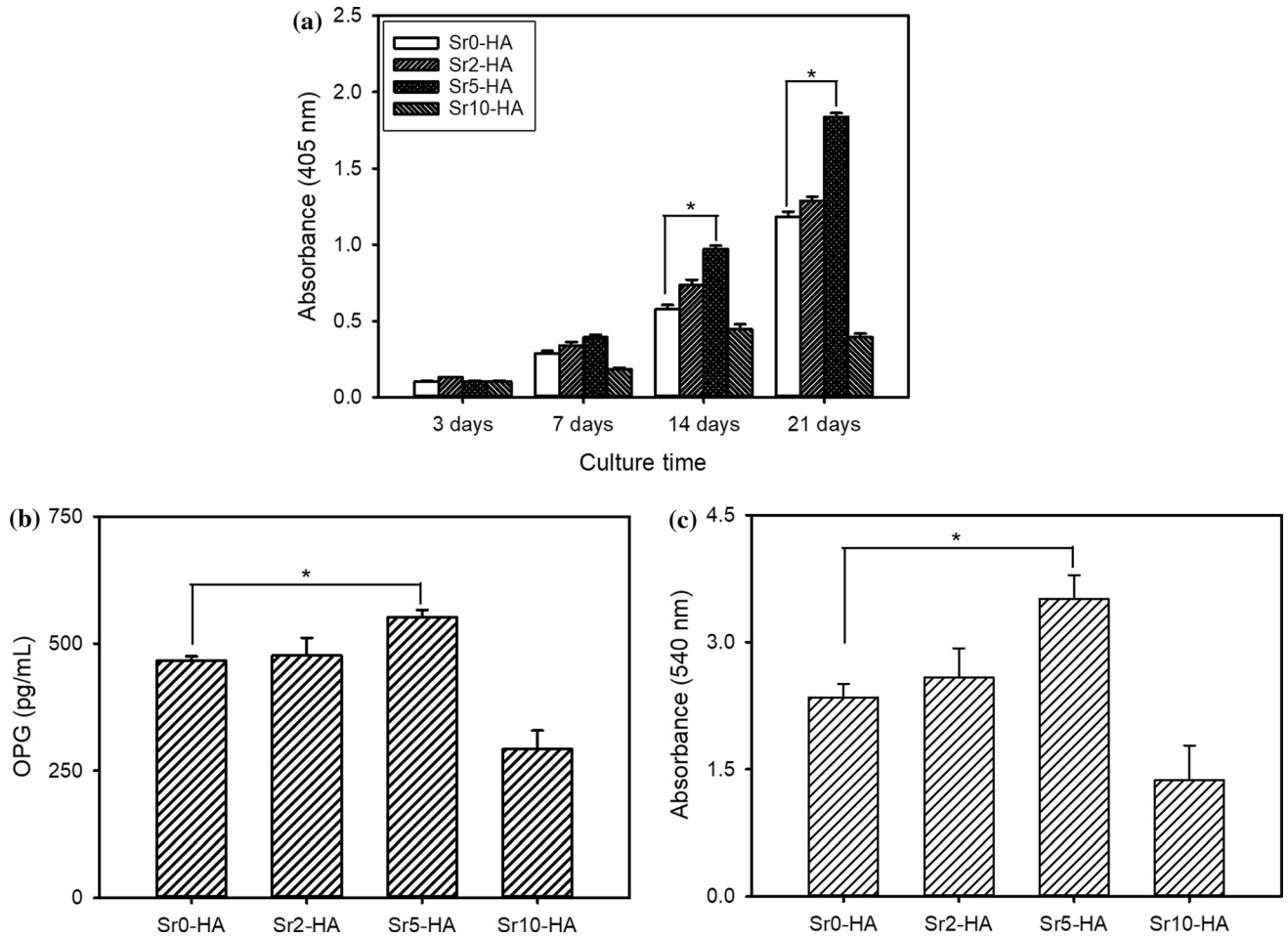

Figure 10 **a** ALP activity of MC3T3-E1 cells on the Sr-HA scaffolds after culturing for 3, 7, 14, and 21 days ($n = 5$). **b** OPG expression of cells on the Sr-HA scaffolds after 7 days of cell culture ($n = 6$) and **c** quantitative calcium deposition of cells on the Sr-HA scaffolds after 14 days of cell culture ($n = 5$). Significant differences from the Sr0-HA scaffold at each time point were denoted as $p^* < 0.05$.

Acknowledgements

This work was supported by research grants from Daegu Catholic University in 2018.

Compliance with ethical standards

Conflict of interest The authors declare that they have no conflict of interest.

References

[1] Wang L, Pathak JL, Liang D, Zhong N, Guan H, Wan M, Miao G, Li Z, Ge L (2020) Fabrication and characterization of strontium-hydroxyapatite/silk fibroin biocomposite nanospheres for bone-tissue engineering. Int J Biol Macromol 142:366–375

[2] Prabha RD, Ding M, Bollen P, Ditzel N, Varma HK, Nair PD, Kassem M (2020) Strontium ion reinforced bioceramic scaffold for load bearing bone regeneration. Mater Sci Eng C 109:110427

[3] Meininger S, Moseke C, Spatz K, März E, Blum C, Ewald A, Vorndran E (2019) Effect of strontium substitution on the material properties and osteogenic potential of 3D powder printed magnesium phosphate scaffolds. Mater Sci Eng C 98:1145–1158

[4] Edwin N, Wilson SSP (2019) Strontium incorporated hydroxyapatite/hydrothermally reduced graphene oxide nanocomposite as a cytocompatibility materials. Ceram Int 45:5475–5485

[5] Zhang W, Shen Y, Pan H, Lin K, Liu X, Darvell BW, Lu WW, Chang J, Deng L, Wang D, Huang W (2011) Effects of strontium in modified biomaterials. Acta Biomater 7:800–808

[6] Shanmugam S, Gopal B (2014) Copper substituted hydroxyapatite and fluorapatite: synthesis, characterization and antimicrobial properties. Ceram Int 40:15655–15662

[7] Nagyné-Kovács T, Studnicka L, Kincses A, Spengler G, Molnár M, Tolner M, Lukács IE, Szilágyi IM, Pokol G (2018) Synthesis and characterization of Sr and Mg-doped hydroxyapatite by a simple precipitation method. Ceram Int 44:22976–22982

[8] Lee JH, Mandakhbayar N, El-Fiqi A, Kim HW (2017) Intracellular co-delivery of Sr ion and phenamil drug through mesoporous bioglass nanocarriers synergizes BMP signaling and tissue mineralization. Acta Biomater 60:93–108

[9] Peng S, Zhou G, Luk KDK, Cheung KMC, Li Z, Lam WM, Zhou Z, Lu WW (2009) Strontium promotes osteogenic differentiation of mesenchymal stem cells through the Ras/MAPK signaling pathway. Cell Physiol Biochem 23:165–174

[10] Zhang J, Wang M, Cha JM, Mantalaris A (2009) The incorporation of 70s bioactive glass to the osteogenic differentiation of murine embryonic stem cells in 3D bioreactors. J Tissue Eng Regen Med 3(1):63–71

[11] Kavitha M, Subramanian R, Vinoth KS, Narayanan R, Venkatesh G, Esakkiraja N (2015) Optimization of process parameters for solution combustion synthesis of strontium substituted hydroxyapatite nanocrystals using design of experiments approach. Powder Technol 271:167–181

[12] Park SY, Kim KI, Park SP, Lee JH, Jung HS (2016) Aspartic acid-assisted synthesis of multifunctional strontium-substituted hydroxyapatite microspheres. Cryst Growth Des 16:4318–4326

[13] Liu D, Nie W, Li D, Wang W, Zheng L, Zhang J, Zhang J, Peng C, Mo X, He C (2019) 3D printed PCL/SrHA scaffold for enhanced bone regeneration. Chem Eng J 362:269–279

[14] Zhang W, Feng C, Yang G, Li G, Ding X, Wang S, Dou Y, Zhang Z, Chang J, Wu C, Jiang X (2017) 3D-printed scaffolds with synergistic effect of hollow-pipe structure and bioactive ions for vascularized bone regeneration. Biomaterials 135:85–95

[15] Raucci MG, Giugliano D, Perez MAA, Ambrosio L (2015) Effects on growth and osteogenic differentiation of mesenchymal stem cells by the strontium-added sol–gel hydroxyapatite gel materials. J Mater Sci Mater Med 26:90–101

[16] Boanini E, Torricelli P, Sima F, Axente E, Fini M, Mihailescu IN, Bigi A (2018) Gradient coatings of strontium hydroxyapatite/zinc β-tricalcium phosphate as a tool to modulate osteoblast/osteoclast response. J Inorg Biochem 183:1–8

[17] Lu X, Bao C, Xu HHK, Pan J, Hu J, Wang P, Luo E (2016) Osteoprotegerin gene-modified BMSCs with hydroxyapatite scaffold for treating critical-sized mandibular defects in ovariectomized osteoporotic rats. Acta Biomater 42:378–388

[18] Ni GX, Shu B, Huang G, Lu WW, Pan HB (2012) The effect of strontium incorporation into hydroxyapatites on their physical and biological properties. J Biomed Mater Res Part B Appl Biomater 100B:562–568

[19] Rajkumar M, Meenakshisundaram N, Rajendran V (2011) Development of nanocomposites based on hydroxyapatite/sodium alginate: synthesis and characterization. Mater Charact 62:469–479

[20] Padmanabhan SK, Haq EU, Licciulli A (2014) Rapid synthesis and characterization of silicon substituted nano hydroxyapatite using microwave irradiation. Curr Appl Phys 14:87–92

[21] Jiang J, Han G, Zheng X, Chen G, Zhu P (2019) Characterization and biocompatibility study of hydroxyapatite coating on the surface of titanium alloy. Surf Coat Technol 375:645–651

[22] Zhu H, Guo D, Zang H, Hanaor DAH, Yu S, Schmidt F, Xu K (2020) Enhancement of hydroxyapatite dissolution through structure modification by Krypton ion irradiation. J Mater Sci Technol 38:148–158

[23] Zhang E, Zou C, Yu G (2009) Surface microstructure and cell biocompatibility of silicon-substituted hydroxyapatite coating on titanium substrate prepared by a biomimetic process. Mater Sci Eng C 29:298–305

[24] Prabha RD, Nair BP, Ditzel N, Kjems J, Nair PD, Kassem M (2019) Strontium functionalized scaffold for bone tissue engineering. Mater Sci Eng C 94:509–515

[25] Naruphontjirakul P, Porter AE, Jones JR (2018) In vitro osteogenesis by intracellular uptake of strontium containing bioactive glass nanoparticles. Acta Biomater 66:67–80

[26] Humphrey EL, Williams JHH, Davie MWJ, Marshall MJ (2006) Effects of dissociate glucocorticoids on OPG and RANKL in osteoblastic cells. Bone 38:652–661